CRUSHING AND FRACTURE ENERGIES IN CONCRETE SPECIMENS MONITORED BY ACOUSTIC EMISSION

G. LACIDOGNA, F. ACCORNERO, M. CORRADO AND A. CARPINTERI

Politecnico di Torino
Department of Structural, Geotechnical and Building Engineering
Corso Duca degli Abruzzi 24, 10129 Torino, Italy
e-mail: giuseppe.lacidogna@polito.it – federico.accornero@polito.it – mauro.corrado@polito.it –
alberto.carpinteri@polito.it

Key words: Compression test, Three-point bending test, Brittle fracture, Energy release, Acoustic Emission.

Abstract: Experimental tests have been carried out to evaluate the crushing and the fracture energies absorbed by concrete specimens during compression and flexural failure. In the former case, concrete cylindrical specimens having a different slenderness have been considered. In order to obtain the complete load vs. displacement response, the tests have been controlled by the circumferential strain measured with a linked chain placed around the cylinder at mid-height. The absorbed energy per surface unit is computed from the overlapping constitutive law. As far as the fracture energy is concerned, three-point bending tests have been carried out according to RILEM recommendations. The loading process has been displacement-controlled, and the fracture energy computed as the area beneath the load vs. mid-span deflection curve. Furthermore, all the tests have been monitored by the Acoustic Emission (AE) technique. In particular, the evolution of the most representative AE parameters has been analyzed, in order to better understand the cracking pattern evolution during the test. The waves frequency and the rise angle are used to discriminate the prevailing cracking mode from pure opening or sliding. The cumulated number of AE events and their amplitude are used to compute the signal energy.

1 INTRODUCTION

Damage and fracture characterizing the compressive failure of heterogeneous materials such as rocks and concrete are complex processes involving wide ranges of time and length scales, from the micro- to the structural-scale. They are governed by the nucleation, growth and coalescence of microcracks and defects, eventually leading to the final collapse, and to the loss of the classical mechanical parameters, such as nominal strength, dissipated energy density and deformation at failure, as material properties [1]. Furthermore, the collapse mechanism is strongly related to the cracking pattern developing during the loading process. It changes from crushing, for very stocky specimens, to shear failure characterized by the formation of inclined slip bands for intermediate values of slenderness, to splitting for very slender specimens.

Such a variety of failure mechanisms makes the definition of scale-invariant mechanical parameters difficult to be achieved. However, according to experimental evidences [2,3], the post-peak phase is characterized by a strong strain localization, independently of the actual collapse mechanism. Consequently, in the softening regime, energy dissipation takes place over an internal surface rather than within a volume, in close analogy with the behavior in tension. According to these

evidences, the overlapping crack model has been proposed by Carpinteri et al. [4] for modeling the compressive behavior of concrete-like materials. Such a model, dual to the cohesive crack model routinely adopted for quasi-brittle materials in tension, assumes a stress vs. displacement (fictitious interpenetration) law as a material property for the post-peak behavior, to which corresponds an energy dissipation over a surface. This simple model has permitted to explain the well-known size and slenderness effects on the structural ductility, characterizing the mechanical behavior of concrete-like materials subjected to uniaxial and eccentric compression tests [4,5].

The overlapping crack model is very effective in describing the overall behavior of specimens in compression, without going into the details of the cracking pattern, as well as in determining the amount of energy dissipated during the complete loading process. On the other hand, more information on the modalities of energy release and the development of cracking patterns can be obtained on the basis of the acoustic emission (AE) monitoring technique, that proves possible to detect the occurrence and evolution of stress-induced cracks. Cracking, in fact, is accompanied by the emission of elastic waves which propagate within the bulk of the material. These waves can be received and recorded by transducers applied to the surface of structural elements. This technique, originally used to detect cracks and plastic deformations in metals, has been extended to studies in the field of rocks and concrete, where it can be used for the diagnosis of structural damage phenomena [6,7]. Recently, AE data have been interpreted by means of statistical and fractal analysis [7], showing that the energy release, proportional to the cumulative number of AE events, is a surface-dominated phenomenon. Analogously, also the localization of cracks distribution within the specimen volume by means of the AE technique has physically confirmed the localization of the energy dissipation over preferential bands and surfaces during the damage evolution [8-10].

In the present paper, crushing and fracture energies of concrete materials are computed from the results of compression and three-point bending tests, respectively. At the same time, they are also derived on the basis of the AE monitoring performed during the tests. Moreover, the type of failure is identified from the analysis of the shape of the AE waves recorded during the tests [11-16].

2 THEORETICAL MODELS

2.1 Uniaxial compression

The overlapping crack model proposed by Carpinteri et al. [4] describes the inelastic deformation due to material damage in the post-peak softening regime by means of a fictitious interpenetration of the material, while the bulk material undergoes an elastic unloading. Such a behavior is described by a couple of constitutive laws in compression, in close analogy with the cohesive crack model: a stress vs. strain relationship for the undamaged material (Fig. 1a), and a stress vs. displacement (fictitious overlapping) relationship describing the material crushing and expulsion (Fig. 1b). The latter law describes how the stress in the damaged material decreases by increasing the interpenetration displacement, up to a residual value, σ_r, is reached, to which corresponds the critical value for displacement, w_{cr}. The area below the stress vs. overlapping displacement curve of Fig. 1b represents the crushing energy, $\mathcal{G}_C$, which can be assumed, under certain hypotheses, as a size-independent material property.
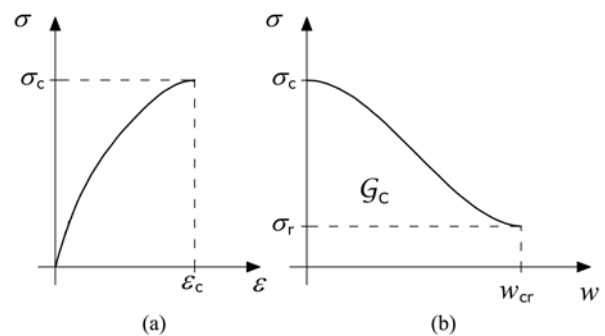

Figure 1: Overlapping Crack Model: (a) pre-peak stress vs. strain diagram; (b) post-peak stress vs. interpenetration law.

2

According to the overlapping crack model, the mechanical behavior of a specimen subjected to uniaxial compression (see Fig. 2) can be described by three schematic stages. A first stage where the behavior is mainly characterized by the elastic modulus of the material: a simple linear elastic stress–strain law can be assumed, or even more complicated nonlinear relationships, taking into account energy dissipation within the volume due to initiation and propagation of microcracks (see Fig. 2b). By approaching the compressive strength, such microcracks interact forming macrocracks, and, eventually, localizing on a preferential surface. A second stage where, after reaching the ultimate compressive strength, σ_c, the inelastic deformations are localized in a crushing band. The behavior of this zone is described by the softening law shown in Fig. 1b, whereas the remaining part of the specimen still behaves elastically (see Fig. 2c). The displacement of the upper side can be computed as the sum of the elastic deformation and the interpenetration displacement w:

$$\delta = \varepsilon l + w \text{ , for } w < w_{cr} \qquad (1)$$

where l is the specimen length. Both ε and w are functions of the stress level, according to the corresponding constitutive laws shown in Fig. 1. While the crushing zone overlaps, the elastic zone expands at progressively decreasing stresses. When $\delta \geq w_{cr}$, in the third stage, the material in the crushing zone is completely damaged and is able to transfer only a constant residual stress, σ_r (see Fig. 2d).

As a result, very different global responses in the σ–δ diagram can be obtained by varying the mechanical and geometrical parameters of the sample. In particular, the softening process is stable under displacement control, only when the slope $d\delta/d\sigma$ in the softening regime is negative, Fig. 3a. A sudden drop in the load bearing capacity under displacement control takes place when the slope is infinite, Fig. 3b. Finally, the snap-back instability is avoided, Fig. 3c, if the loading process is controlled by means of the localized interpenetration or the circumferential strain, the slope $d\delta/d\sigma$ of the softening branch being positive. Analogously

to quasi-brittle materials subjected to tension, the stability of the overall behavior of specimens in compression depends on geometrical (size and slenderness) and mechanical parameters (crushing energy, compressive strength and ultimate strain). In accordance with previous studies proposed by the authors in [5], a catastrophic softening (snap-back) occurs when:

$$\frac{s_{E,c}}{\varepsilon_c \lambda} \leq \frac{1}{2.3} \qquad (2)$$

where $\lambda = l/d$ is the specimen slenderness, ε_c is the elastic strain recovered during the softening unloading, and

$$s_{E,c} = \frac{\mathcal{G}_C}{\sigma_c d} \qquad (3)$$

is the energy brittleness number in compression, proposed by Carpinteri et al. [5].
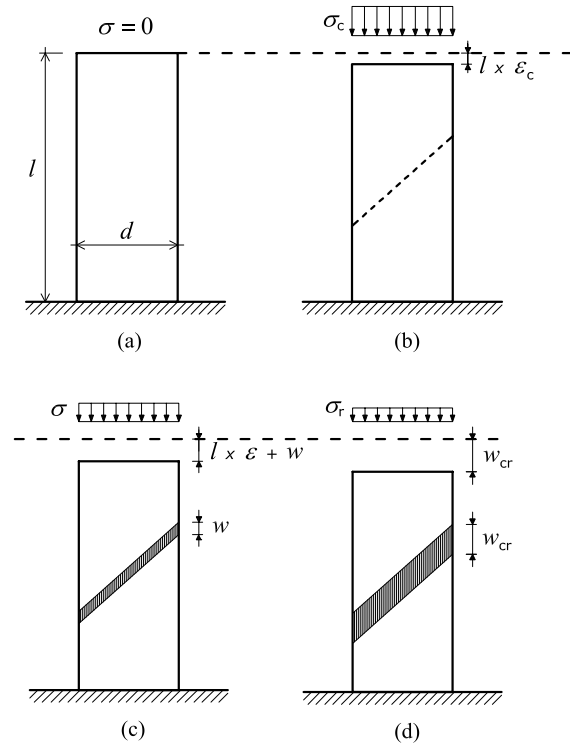

Figure 2: Subsequent stages in the deformation history of a specimen in compression.

(a) Normal softening

(b) Vertical drop

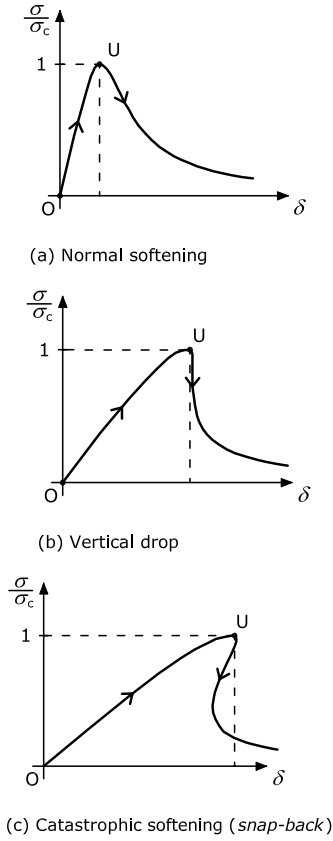(c) Catastrophic softening (*snap-back*)

Figure 3: Stress vs. displacement response of a specimen in compression.

An extended validation of the overlapping crack model for concrete-like materials can be found in Carpinteri et al. [5], where specimens of different materials as well as different slenderness and/or size have been considered. For example, the overlapping laws obtained from the results of the compression tests on specimens with different sizes and slendernesses carried out by Ferrara and Gobbi [17] are shown in Fig. 4. The post-peak regime in the stress vs. strain response is largely influenced by the slenderness and the scale of the specimen (Fig. 4b), whereas the stress vs. displacement curves collapse onto a very narrow band (see fig. 4c), demonstrating that the σ–w relationship is able to provide a slenderness and size-scale independent constitutive law.
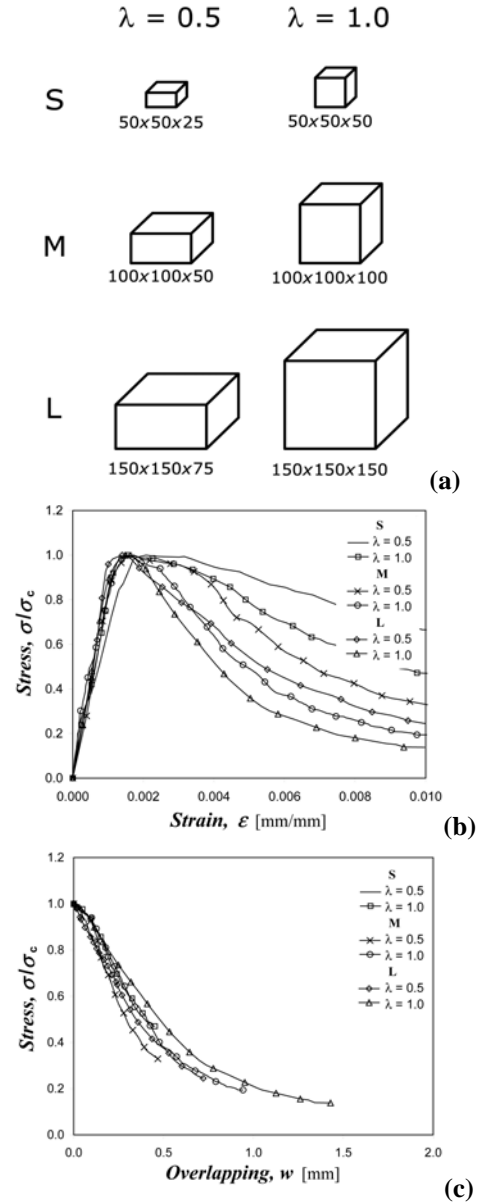

Figure 4: Compression tests on concrete specimens: (a) specimens geometry; (b) stress vs. strain diagrams; (c) overlapping law diagrams.

However, it is to be noted that the overlapping crack model, considered as a scale-invariant constitutive model, is no longer valid when the collapse mechanism significantly changes. In this case, the cracking pattern and the amount of energy dissipation also change significantly. As an example, the shear collapse mechanism determines an high energy dissipation due to friction phenomena spread within the specimen volume. On the contrary, the splitting failure, typical of slender specimens, gives rise to a lower energy dissipation, due to the propagation of a main

longitudinal tensile crack. The stability of the compression phenomenon is still governed by Eq. (2), although the crushing energy depends on the failure mechanism.

2.2 Three-point bending

From a theoretical point of view, the three-point bending test of plain concrete beams can be described by means of the cohesive crack model. A linear-elastic behavior is assumed for the beam up to the maximum tensile stress in the central cross section reaches the ultimate strength. Then, a cohesive crack starts to propagate from the soffit to the extrados of the beam, whereas the rest of the body exhibits an elastic unloading. However, due to the complexity of the process, only the initial linear elastic behavior and the limit case of central cross section completely cracked can be analytically studied (see Fig. 5) [18]. More in details, a linear load vs. deflection relationship is obtained for the former phase, whereas a more complex curve characterizes the post-peak softening phase (Fig. 6). Analogously to the compression test, the stability of the loading process is governed by a nondimensional parameter. Unstable behavior and catastrophic events are expected when [18]:

$$\frac{s_{E,t}}{\varepsilon_u \lambda} \leq \frac{1}{3} \qquad (2)$$

where $\lambda = l/d$ is the beam slenderness, ε_u is the ultimate strain in tension, and $s_{E,t}$ is the energy brittleness number in tension, proposed by Carpinteri [18]. The system is brittle for low brittleness number, high ultimate strain and large slenderness (Fig. 6).
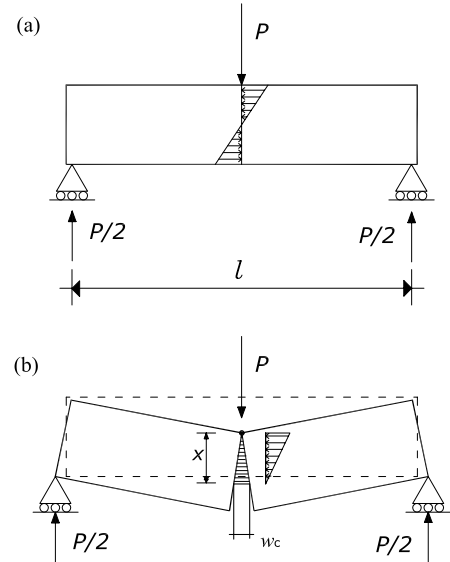

Figure 5: Three-point bending geometry: (a) linear elastic phase; (b) limit situation of complete fracture with cohesive forces.
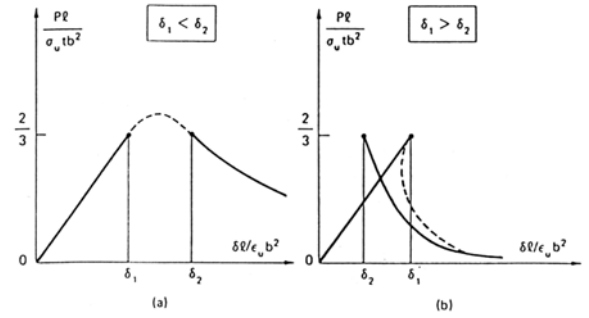

Figure 6: Load–deflection diagrams: (a) ductile; (b) brittle condition ($\delta_1 = \lambda^3/6$; $\delta_2 = s_{E,t}\lambda^2/2\varepsilon_u$).

3 ACOUSTIC EMISSION

The estimation of active cracks is of significant importance for any structural inspection. For an early warning of crack nucleation, the classification of active cracks is a great deal of the AE technique [11].

AE signals due to microcracks are detected by AE sensors attached on the surface of the concrete specimen. The signal waveforms are recorded by the AE measurement system. In order to classify active cracks, AE parameters such as rise time and peak amplitude of each signal are considered to calculate the rise angle (RA) value, defined as the ratio of the rise time (expressed in ms) to the peak amplitude (expressed in V) [11-15].

5

The shape of the AE waveforms is typical of the fracture mode (Fig. 7). Shear events are characterized by long rise times and usually high amplitudes [16,19,20], whereas low rise time values are typical of tensile crack propagations [19,20]. These conditions are synthesized by the RA value [14,15].

Another parameter used to characterize the cracking mode is the Average Frequency (AF) expressed in kHz. The AF values are obtained from the AE ringdown count divided by the duration time of the signal. The AE ringdown count corresponds to the number of threshold crossings within the duration time. In general, the shift from higher to lower values of AF could indicate the shift of the cracking mode from tensile to shear [16]. Nevertheless, when a cracking process involves the opening of large cracks (Mode I), the frequency attenuation must be a function of this discontinuity. In other words, in this case the wavelength of the AE signals needs to be larger for the crack opening to be overcome, and the shift of the frequencies from higher to lower values could support also a dominant tensile cracking mode [7,21].
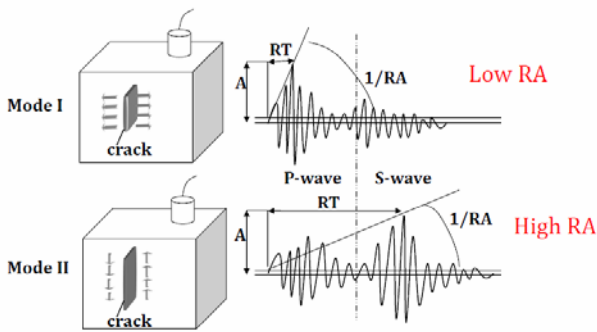

Figure 7: Typical waveforms of tensile and shear events. *A* is the amplitude and RT the rise time (time between the onset and the point of maximum amplitude) of the waveforms [22].

4 EXPERIMENTAL TESTS

4.1 Uniaxial compression

In this section, the results of compression tests carried out on two cylindrical specimens having diameter equal to 100 mm, and slenderness equal to 1.0 and 2.0 are presented (Fig. 8a). The loading process has been controlled by the circumferential strain, measured by means of a linked chain placed around the cylinder at mid-height. Such a control has permitted to completely detect the load–displacement curve, even in case of severe unstable phenomena such as snap-back. More in details, the tests have been controlled by the circumferential strain up to the maximum displacement for the extensometer. Then, the test control has been switched to the piston stroke. During the tests, each specimen has been monitored by the acoustic emission technique. The AE events emerging from the compressed specimens were detected by applying to the sample surface a piezoelectric (PZT) transducer, sensitive in the frequency range from 50 to 800 kHz for detection of high-frequency AEs.

The load vs. circumferential expansion and the load vs. axial displacement curves for the two considered specimens are shown in Fig. 8b,c. According to the expectations, the more slender specimen has exhibited a more brittle behavior, the post-peak branch being almost vertical compared to that of the other specimen, characterized by a normal softening response. However, the two failure mechanisms were very different: a shear failure with several slip bands characterizes the specimen with slenderness equal to 1.0, whereas a splitting failure is obtained for the specimen with slenderness equal to 2.0. As a consequence, the obtained overlapping laws are also very different (see Fig. 8d). The crushing energies are $G_C = 91$ N/mm for the specimen with $\lambda = 1.0$, and $G_C = 43$ N/mm for the specimen with $\lambda = 2.0$. The corresponding values for the total dissipated energy are: 714 J ($\lambda = 1.0$) and 337 J ($\lambda = 2.0$), respectively.

As regards the AE monitoring, the signals were detected by piezoelectric dedicated sensors produced by LEANE NET (Italy). The sampling frequency of recording waveforms was set to 1 Msample/s. The data were collected by a National Instruments digitizer capable up to 8 channels AE sensors. The AE waves, captured by the sensors, were amplified with 60 dB gain before they have been processed, setting the acquisition threshold

level up to 2 mV. The AE sensors were attached to the surface of the specimens with a silicon glue, to guarantee a good contact between the sensor and the specimen, also during the final stages of the test.
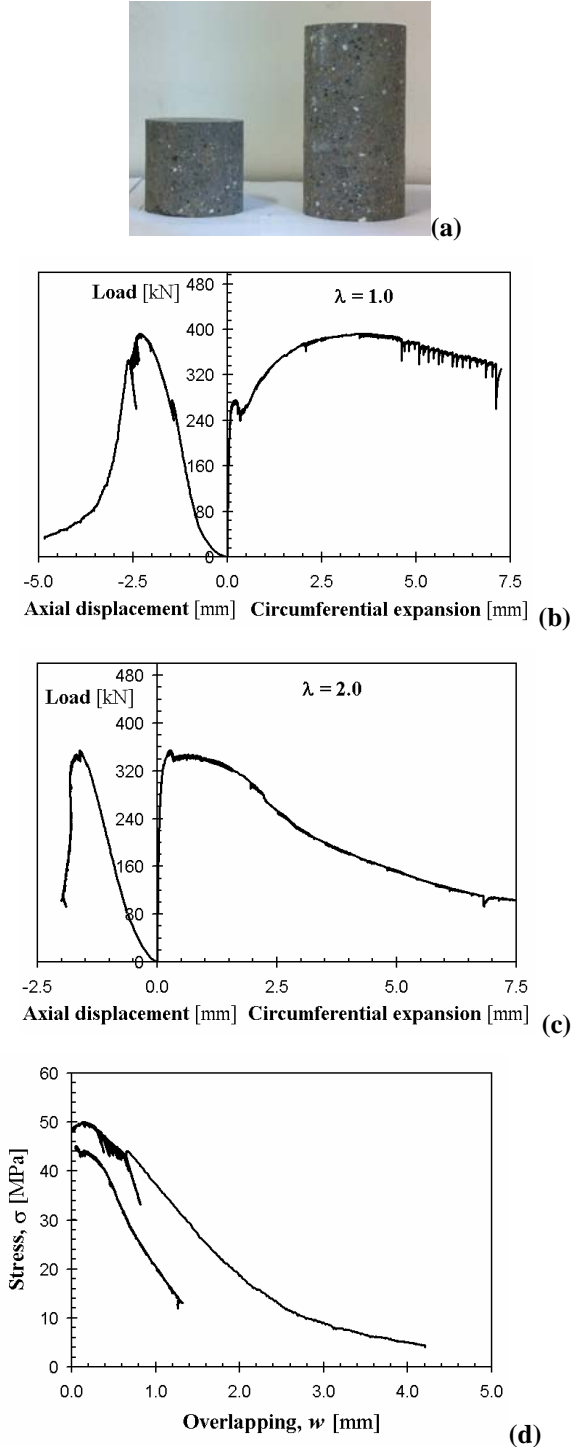

(a)

(b)

(c)

(d)

Figure 8: Compression tests: (a) specimens geometry; load vs. axial displacement and load vs. circumferential expansion curves for (b) λ=1.0, and (c) λ=2.0; (d) corresponding overlapping laws.

The load vs. time diagram of the specimen with slenderness λ = 1.0 is shown in Fig. 9a. During the test a clear increase in the AE events was obtained approaching the peak load (Fig. 9b). The AE average frequencies decrease from 230 kHz to 190 kHz during the loading test. The load process involves a small shift in frequencies from higher to lower values (Fig. 10a) and a significant increase in RA values after the peak load is come out (Fig. 10b). Therefore a dominant presence of shear cracks seems to lead the damage evolution up to the final collapse. The analysis of the energy content obtained by the AE signals (Fig. 10c), calculated as proportional to the envelope of the signal waveform [12], verifies that the damage evolution carries more powerful signals after the peak load, when the final collapse is approaching. During this test, the amount of released AE signals energy is estimated as 1460 ms·V·10^3.

As regards the specimen with slenderness λ=2.0, the cumulative number of AE events at the end of the test is lower than the previous case (see Fig. 11b compared to Fig. 9b). The AE average frequencies decrease from 100 kHz to 50 kHz during the loading test (Fig. 12a). The loading process involves a shift in frequencies from higher to lower values and a significant decrease in RA values after the peak load (Fig. 12b). Therefore a dominant presence of tensile cracks seems to lead the damage evolution up to the final collapse. Due to the slenderness of the specimens and the failure mode shown during the experiment (a single large subvertical crack), the shift in frequencies tends to very low values. As a matter of fact, for high frequency waves it is possible to propagate only through small inhomogeneities, whereas low frequency waves can propagate also through large inhomogeneities [7,21]. From the analysis of the energy content obtained from AE signals (Fig. 12c), also in this case it is verified that the damage evolution carries more powerful signals after the peak load. The amount of released AE signals energy at the end of the test, estimated as 680 ms·V·10^3, is lower than the previous case.
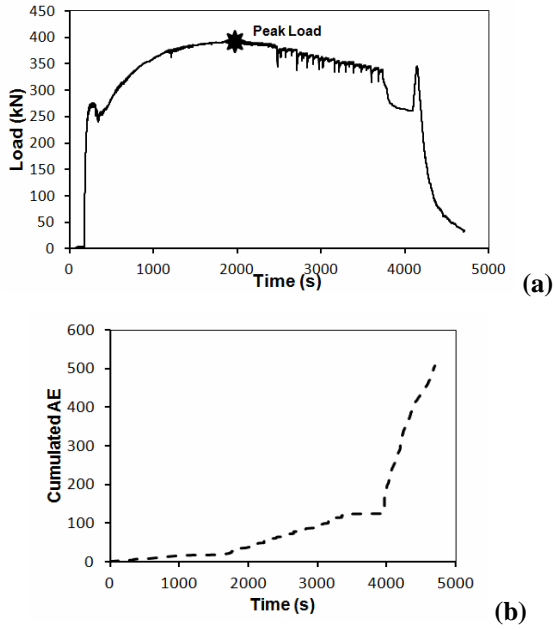
Figure 9: Concrete specimen with slenderness λ=1.0:
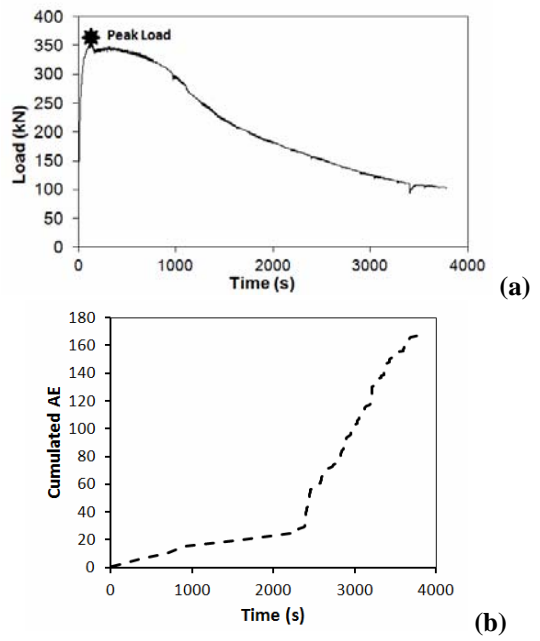(a) load vs. time; (b) cumulated AE events vs. time.

Figure 11: Concrete specimen with slenderness λ=2.0:
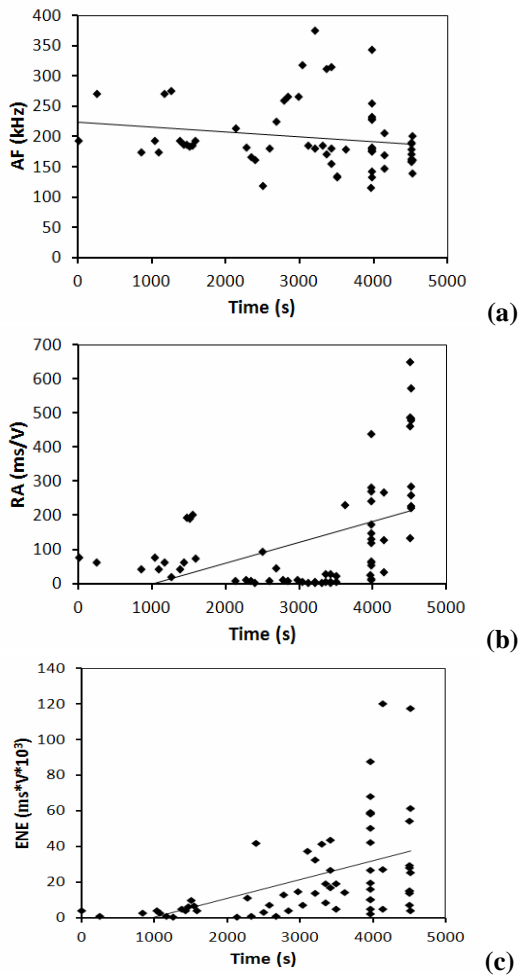(a) load vs. time; (b) cumulated AE events vs. time.

Figure 10: Concrete specimen with slenderness
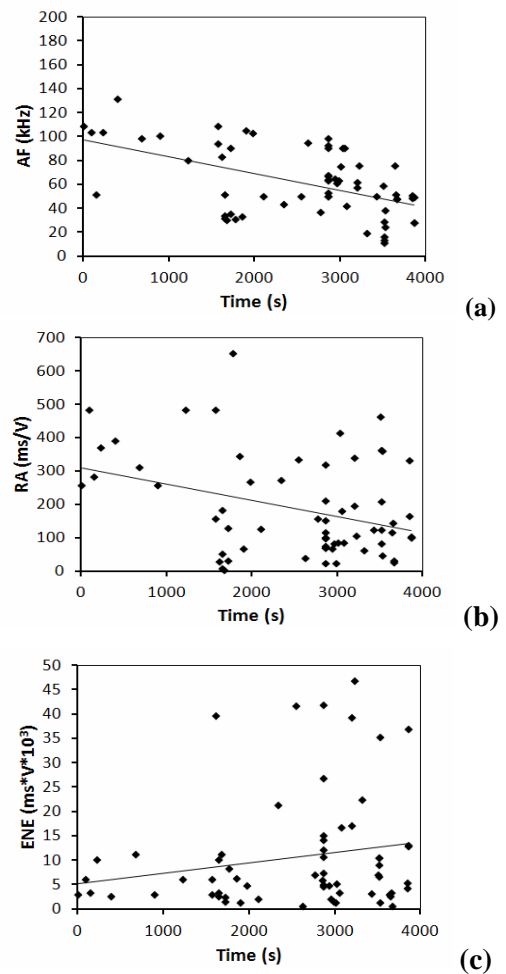λ=1.0: (a) AF values vs. time; (b) RA values vs. time;
(c) AE signal energy vs. time.

Figure 12: Concrete specimen with slenderness
λ=2.0: (a) AF values vs. time; (b) RA values vs. time;
(c) AE signal energy vs. time.

8

4.2 Three-point bending

The results of the three-point bending test performed on a beam having dimensions 100x100x840 mm (Fig. 13a) are herein reported. From the mechanical point of view, the overall behavior is characterized by a normal softening post-peak phase, as shown in Fig. 13b. The fracture energy, evaluated according to the RILEM recommendations [23], is equal to 0.124 N/mm. The corresponding total dissipated energy is equal to 0.62 J.

The AE signals detected from an array of six sensors show characteristics similar to those of the specimen with slenderness $\lambda=2.0$ subjected to compression test. The AE average frequencies range between 180 kHz and 150 kHz (Fig. 15a). A shift in frequencies from higher to lower values (Fig. 15a) and a significant decrease in RA values (Fig. 15b) after the peak load are observed (Fig. 14b). The evolution of the damage from the initial notch towards a Mode I crack is proved both by the RA and the AF decrease, as in the case of the specimen with slenderness $\lambda=2.0$ in compression.
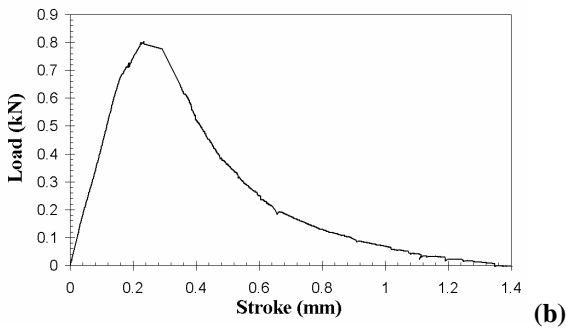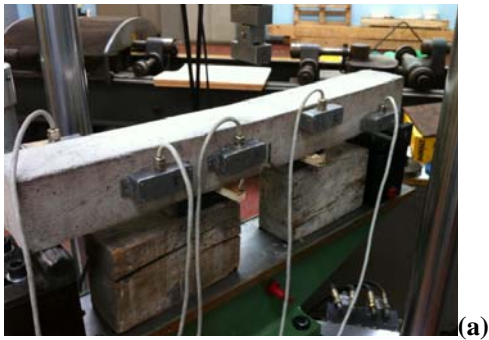

(a)

(b)

Figure 13: Three-point bending test: (a) experimental setup; (b) load vs. deflection curve.
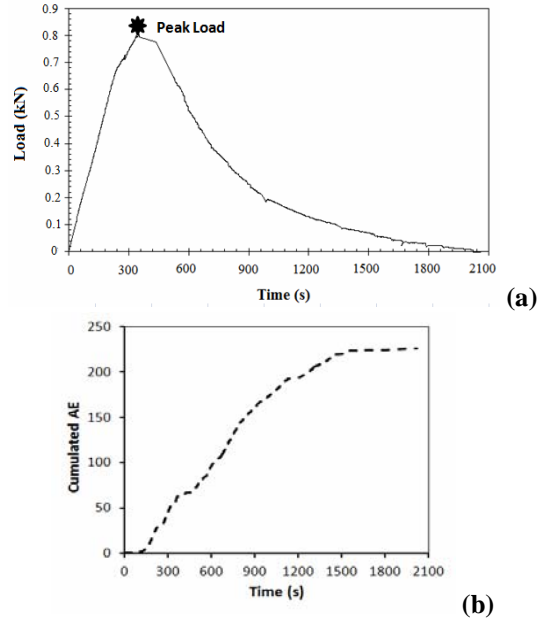

(a)

(b)

Figure 14: Three-point bending test: (a) load vs. time; (b) cumulated AE events vs. time.
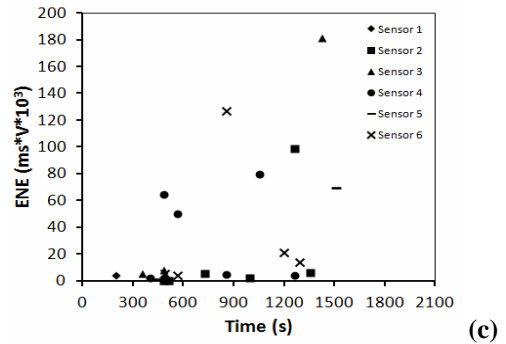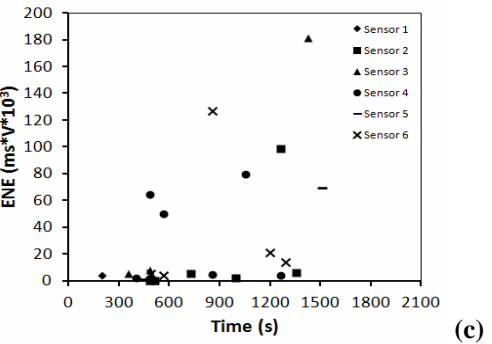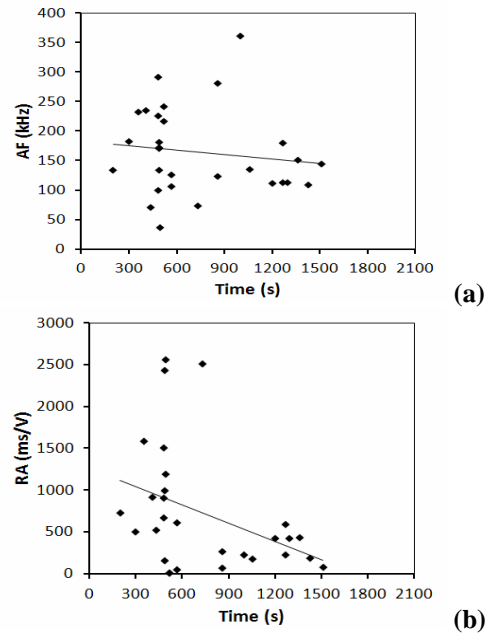

(a)

(b)

(c)

Figure 15: Three-point bending test: (a) AF values vs. time; (b) RA values vs. time; (c) AE signal energy vs. time.

9

The RA values obtained from the three-point bending test are considerably higher than the previous two cases, because of the bigger specimen size: as a matter of fact the additional propagation distance from AE sources to sensors, considering attenuation mechanisms, involves an increase in AE signals rise time [22]. Since the longitudinal waves are the fastest type, the delay in each AE signal between longitudinal and shear waves grows with the increasing of the propagation length, and consequently the RA raises from lower to higher values.

The signal energy of the AE events detected during the test are reported in Fig. 16c, distinctly for each sensor. The average value of the total released AE signals energy is estimated as 126 ms·V·10^3.

6 CONCLUSIONS

The AE results obtained from compression and three-point bending tests, prove that the variation of the AE parameters during the loading process strictly depends on the specimen damage: a decrease in frequency may be provoked both by dominant shear cracking process and by dominant tensile cracking process. Therefore, the two different cracking modes have to be discriminated through a different AE parameter, such as the rise angle (RA), that is defined as the ratio of the rise time to the peak amplitude of each signal. Low RA values suggest a Mode I crack propagation, whereas high RA values are obtained in case of Mode II crack propagation. All the monitored damage processes display an increase in AE signal energy content approaching the final failure.

The values of the total dissipated energy for the specimens subjected to compression are 714 J for λ=1.0 and 337 J for λ=2.0, with a ratio of 2.11 about. An analogous result is obtained for values of the AE signals energy (in this case the ratio is 2.14), suggesting the possibility to define a correlation between the two parameters. On the contrary, the fracture energy derived from the three-point bending test is about 3 orders of magnitude lower than the crushing energy, whereas the AE signals

energy related to the flexural failure is only one order of magnitude lower than that relative to the compression failure. This suggests the impossibility to define a unique correlation between AE signal energy and mechanical dissipated energy, independently of the failure mode. In order to better substantiate these outcomes, the authors are carrying on further experimental tests, both in compression and flexure, on specimens with different size and slenderness.

AKNOWLEDGEMENTS

REFERENCES

[1] Carpinteri, A., Corrado, M. and Lacidogna G., 2012. Three different approaches for damage domain characterization in disordered materials: Fractal energy density, *b*-value statistics, renormalization group theory. *Mechanics of Materials*, **53:**15-28.

[2] Kotsovos, M.D., 1983. Effect of testing technique on the post-ultimate behaviour of concrete in compression. *Mater. Struct.* **16**:3-12.

[3] Van Mier, J.G.M., 1984. *Strain softening of concrete under multiaxial compression.* PhD Thesis, Eindhoven University of Technology, The Netherlands.

[4] Carpinteri, A., Corrado, M., Mancini, G. and Paggi, M., 2009. The overlapping crack model for uniaxial and eccentric concrete compression tests. *Mag. Concr. Res.* **61**:745-57.

[5] Carpinteri, A., Corrado, M. and Paggi, M., 2011. An analytical model based on strain localization for the study of size-scale and slenderness effects in uniaxial compression tests. *Strain* **47**:351-62.

[6] Ohtsu, M., The history and development of acoustic emission in concrete engineering. *Mag. Concr. Res.* **48**:321-30.

[7] Carpinteri, A., Lacidogna, G. and Pugno, N., 2007. Structural damage diagnosis and life-time assessment by acoustic emission

monitoring. *Eng. Fract. Mech.* **74**:273-89.

[8] Carpinteri, A., Lacidogna, G., Niccolini, G. and Puzzi,S., 2008. Critical defect size distributions in concrete structures detected by the acoustic emission technique. *Meccanica* **43**:349-63.

[9] Carpinteri, A., Lacidogna, G. and Puzzi, S., 2008. Prediction of cracking evolution in full scale structures by the b-value analysis and Yule statistics. *Phys. Mesomech.* **11**:260-71.

[10] Weiss, J. and Marsan, D., 2003. Three-dimensional mapping of dislocation avalanches: clustering and space/time coupling. *Science* **299**:89-92.

[11] C. Grosse and M. Ohtsu, "Acoustic Emission Testing", Springer (2008).

[12] RILEM Technical Committee TC212-ACD, 2010. Acoustic Emission and related NDE techniques for crack detection and damage evaluation in concrete: Measurement method for acoustic emission signals in concrete. *Mater. Struct.*, **43**:1177-81.

[13] RILEM Technical Committee TC212-ACD, 2010. Acoustic Emission and related NDE techniques for crack detection and damage evaluation in concrete: Test method for damage qualification of reinforced concrete beams by Acoustic Emission. *Mater. Struct.* **43**:1183-6.

[14] RILEM Technical Committee TC212-ACD, 2010. Acoustic Emission and related NDE techniques for crack detection and damage evaluation in concrete: Test method for classification of active cracks in concrete by Acoustic Emission. *Mater. Struct.* **43**:1187-9.

[15] RILEM Technical Committee TC212-ACD, 2010. *Acoustic Emission and Related Non-destructive Evaluation Techniques for Crack Detection and Damage Evaluation in Concrete*. Final Report of RILEM Technical Committee 212 ACD.

[16] Ohno, K. and Ohtsu, M., 2010. Crack classification in concrete based on Acoustic Emission. *Constr. Build. Mater.* **24**:2339-46.

[17] Ferrara, G. and Gobbi, M.E., 1995. *Strain softening of concrete under compression*. Report to RILEM Committee 148 SCC, ENEL-CRIS Laboratory, Milano, Italy.

[18] Carpinteri, A., 1989. Size effects on strength, toughness, and ductility, *J. Eng. Mech.* **115**:1375-92.

[19] Soulioti, D., Barkoula, N.M., Paipetis, A., Matikas, T.E., Shiotani T. and Aggelis, D.G., 2009. Acoustic Emission behavior of steel fibre reinforced concrete under bending. *Constr. Build. Mater*. **23**:3532-6.

[20] Aggelis, D.G., 2011. Classification of cracking mode in concrete by Acoustic Emission parameters. *Mech. Res. Communications* **38**:153-7.

[21] Landis, E.N. and Shah, S.P., 1995. Frequency-dependent stress wave attenuation in cement-based materials. *J. Eng. Mech.* **121**:737-43.

[22] Aggelis, D.G., Mpalaskas A.C., Ntalakas D. and Matikas T.E., 2012. Effect of wave distortion on acoustic emission characterization of cementitious materials. *Construction and Building Materials,* **35**:183-190.

[23] RILEM 50-FMC Committee, 1986, Determination of the fracture energy of mortar and concrete be means of three-point bend tests on notched beams. *Mater. Struct.* **18**:286-90.